pH-Dependent Conformational Changes in Tear Lipocalin by Site-Directed Tryptophan Fluorescence

ARTICLE *in* BIOCHEMISTRY · DECEMBER 2009

Impact Factor: 3.02 · DOI: 10.1021/bi901435q · Source: PubMed

3 AUTHORS, INCLUDING:

Oktay K Gasymov
University of California, Los Angeles
49 PUBLICATIONS **938** CITATIONS

SEE PROFILE

Published in final edited form as:
Biochemistry. 2010 January 26; 49(3): 582–590. doi:10.1021/bi901435q.

PH-dependent Conformational Changes in Tear Lipocalin by Site Directed Tryptophan Fluorescence

Oktay K. Gasymov, **Adil R. Abduragimov**, and **Ben J. Glasgow***
Departments of Pathology and Ophthalmology, UCLA School of Medicine, Jules Stein Eye Institute, 100 Stein Plaza, Los Angeles CA 90095, USA

Abstract

Tear lipocalin (TL), a major protein of human tears, binds a broad array of endogenous ligands. PH-dependent ligand binding in TL may have functional implications in tears. Previously, conformational selections of the loops AB and GH have been implicated in ligand binding by site-directed tryptophan fluorescence (SDTF). In this study, SDTF was applied on the loops AB and GH to investigate pH-driven conformational changes relevant to ligand binding. Both loops demonstrate significant but distinct conformational rearrangements over a wide pH range. In the low pH transition, from 7.3 to 3.0, residues of the loop GH show the decreased solvent accessibilities. In acrylamide quenching experiments, the average quenching rate constant (k_q, accessibility parameter) of the residues in the loop GH is decreased about 38%, from 2.1×10^9 $M^{-1}s^{-1}$ to 1.3×10^9 $M^{-1}s^{-1}$. However, despite the significant changes in accessibilities for some residues in the loop AB, the average accessibility per residue remained unchanged (average k_q= 1.2 $M^{-1}s^{-1}$). Accordingly, low pH transition induces conformational changes that reshuffle accessibility profiles of the residues in the loop AB. A significant difference in the titration curves between holo- and apo-forms of W28 mutant suggests that the protonation states of the residues around the position 28 modulate conformational switches of the loop AB relevant to ligand binding.

Tear lipocalin (TL), also known as von Ebner's gland protein, is a prominent member of lipocalin family. As a typical lipocalin, TL possesses a ligand binding barrel that consists of eight antiparallel β- strands with a repeated +1 topology (1). The solution structure of TL, determined by site-directed tryptophan fluorescence (SDTF), has revealed a capacious cavity (2). These findings have subsequently been verified by crystallography (3).

TL is the principal lipid binding protein in tears and the second most abundant protein by molarity. TL binds a broad array of endogenous ligands that include an assortment of fatty acids, alkyl alcohols, glycolipids, phospholipids and cholesterol (4). Numerous putative functions have been suggested for TL. These are scavenging lipid from the corneal surface to prevent the formation of lipid induced dry spots (5), solubilization of lipid in tears (2), antimicrobial activity (6), cysteine proteinase inhibition(7), transport of sapid molecules in saliva (8), transport of retinol in tears (9), scavenging potentially harmful lipid oxidation products (10), transport of antioxidants in tears (11), and endonuclease activity (12).

Because all putative functions of TL are linked to various ligands, molecular mechanisms of ligand binding are of considerable interest. Commonly, a single binding site is presumed for ligand binding to a protein. TL demonstrates a different motif. Spin labeled analogs of fatty acids have been used to determine the orientation of fatty acids in the cavity of TL. Fatty acids

*Corresponding author: Ben J. Glasgow Departments of Pathology and Ophthalmology, UCLA School of Medicine, Jules Stein Eye Institute, 100 Stein Plaza, Rm# B269, Los Angeles CA 90095, USA Phone: (310) 825-6998 Fax: (310) 794-2144 bglasgow@mednet.ucla.edu.

are oriented with the hydrocarbon tail buried in the cavity and the carboxyl group oriented toward the mouth (13,14). However, TL can also interact, although relatively weakly, with fatty acids oriented in the opposite direction. SDTF was applied to measure the ligand binding energy landscape of TL (15). Palmitic acid does not have a single position, but is distributed asymmetrically in the cavity of TL. Experimental data suggest that the ligand binding selects the excited protein states, which originate primarily from conformational selections of the loops AB and GH (15). The loops AB and GH are not resolved in crystal structure (3). Since, the crystal structure of TL was determined at 100K, the low electron density observed for the loops AB and GH most likely arises from the trapped conformational substates, whose coordinates deviate significantly from each other.

In protein binding to small ligands, a population-shift to the active conformations (excited protein states) rather than an induced-fit mechanism is dominant (16). This mechanism was also suggested for binding of fatty acids to β-lactoglobulin, which belongs to the lipocalin family. It has been well documented that the active conformation of β-lactoglobulin originates from fluctuation of the protonation states of Glu89 that create “open” or “closed” forms of the protein (17–21). Therefore, the conformational states of β-lactoglobulin can be modulated by changing the pH of the solution.

Changes in pH, along with those in temperature, pressure, and chemical milieu are widely employed to populate excited protein states. In addition, pH-dependent ligand binding may be functionally important for TL because the tear film is replete with negatively charged lipids that potentially create a steep pH gradient at lipid-water interfaces (22). PH-driven structural rearrangements as well as perturbations in ligand binding have been shown for TL (23–26). PH-dependent ligand binding has been demonstrated for other lipocalins, such as retinol binding protein (27,28), nitrophorin (29), and the membrane enzyme PagP (30). Conformational rearrangements, mainly involving the loops at the open end of the calyx, are considered to be a general feature of the ligand binding mechanism of the lipocalins (21).

Despite the fact that above mentioned lipocalins share the same pH-dependent feature in ligand binding, details of the molecular actions and outcomes are different. In TL, the movement of the opposing loops CD and EF, which influence the ligand binding, is regulated by pH (24). However, application of SDTF to TL reveals that the loops GH and AB (the longest loop in lipocalin family) have decisive roles in ligand binding. Also, these loops have been thought to participate in both conformational selection of the excited protein states and direct interaction with the ligand (15).

In this study, SDTF was applied to the loops AB and GH to investigate pH-driven conformational changes. Both loops, AB and GH, of TL demonstrate significant conformational rearrangements over a wide pH range. Saturation of TL with palmitic acid alters pH-induced conformational changes for some tested positions. These imply that fluctuations between protonated and unprotonated states of amino acids of TL induce conformational changes necessary for ligand binding.

MATERIALS AND METHODS

Materials

Acrylamide and other chemicals used to prepare various buffers were purchased from Sigma-Aldrich (St. Louis, MO).

Site-directed mutagenesis and plasmid construction

The TL cDNA in PCR II (Invitrogen), previously synthesized (31), was used as a template to clone the TL gene spanning bases 115–592 of the previously published sequence (9) into pET

20b (Novagen, Madison, WI). Flanking restriction sites for NdeI and BamHI were added to produce the native protein sequence as found in tears but with the addition of an initiating methionine (32). To construct mutant proteins with a single tryptophan, the previously well characterized TL mutant, W17Y, was prepared with oligonucleotides (Universal DNA Inc., Tigard, OR) by sequential PCR steps (33,34). Using this mutant as a template, mutant cDNAs were constructed in which selected amino acids were additionally substituted with tryptophan or cysteine. Amino acid 1 corresponds to His, bases 115–118 according to Redl (9).

To characterize pH induced conformational transitions in TL, 17 single Trp mutants that cover the loops AB and GH at the open end of the cavity were tested (Figure 1). W17Y mutant, which has been characterized previously (34), was used as a template. Single Trp mutants of TL include W17Y/D25W (for simplicity denoted as W25); W17Y/R26W (W26); W17Y/E27W (W27); W17Y/F28W (W28); W17Y/P29W (W29); W17Y/E30W (W30); W17Y/M31W (W31); W17Y/N32W (W32); W17Y/L33W (W33); W17Y/E34W (W34); W17Y/S35W (W35); W17Y/V36W (W36); W17Y/T37W (W37); W17Y/H106W (W106); W17Y/G107W (W107); W17Y/K108W (W108); W17Y/P109W (W109). All mutant proteins have the native fold, which have previously been characterized by far-UV circular dichroism. In addition, all mutant proteins show similar ligand binding properties, which is the principal function of native TL in tears (15).

Expression and purification of mutant proteins

The mutant plasmids were transformed in E. Coli, BL 21 (DE3) and cells were cultured and proteins were expressed, purified, and analysed as described in the supporting information (2,24). The expressed mutant proteins were used as apo-proteins. To obtain the holo-proteins, apo-proteins were enriched with palmitic acid (1:2).

Absorption Spectroscopy

UV absorption spectra were measured at room temperature using Shimadzu UV-2400PC spectrophotometer.

CD spectral measurements

Spectra were recorded (Jasco 810 spectropolarimeter, 0.2 and 10 mm path length for far- and near-UV spectra, respectively, using protein concentrations of 1.2 mg/ml in 10 mM sodium phosphate (pH 7.5–5.5) or 30mM sodium citrate (pH 4.0–3.0). Eight and sixteen scans from 190–260 nm and 250–320 nm were averaged, respectively. Results were recorded in mdegrees and converted to mean residue ellipticity in $\mathrm{deg}\cdot \mathrm{cm}^{2}\cdot \mathrm{dmol}^{-1}$.

The biuret and the Lowry methods were used to determine protein concentrations of stock and dilute solutions, respectively (35,36).

Steady-state fluorescence spectroscopy

Steady-state fluorescence measurements were made on a Jobin Yvon-SPEX (Edison, NJ) Fluorolog tau-3 spectrofluorometer, the bandwidths for excitation and emission monochromators were 2 nm and 3 nm, respectively. The excitation λ of 295 nm was used to ensure that fluorescence emitted only from the tryptophanyl groups. Protein solutions with about 0.05 OD at 295 nm were analyzed. All spectra were obtained from samples in 10 mM sodium phosphate (pH 7.5–5.5) or 30mM sodium citrate (pH 4.0–3.0) at room temperature. The fluorescence spectra were corrected for light scattering from buffer. Each fluorescence λ_{max} value was determined as an average of five measurements.

Fluorescence lifetime measurements

The fluorescence intensity decays were measured using a LaserStrobe™ fluorescence lifetime instrument (Photon Technology International, Inc., Birmingham, NJ), which consists of a nitrogen laser (GL-3300) linked to a dye laser (GL 302), a frequency doubler (GL 303) and a stroboscopic detector. Laser light with a wavelength of 295 nm was obtained from frequency doubling of 590 nm light using Rhodamine 6G (Exciton, Inc, Dayton, Ohio, USA) dye solution. The 295 nm pulses (fwhm ~ 1.5 ns) were used for the excitation of the single Trp mutants. The decay curves were analyzed at the wavelengths of the respective emission maxima. The emission monochromator slit was 3–5 nm. All measurements were conducted at room temperature. The IRF was determined by measuring scattered light from a solution of glycogen. A DPU-15 optical depolarizer (Optics for Research, Caldwell, NJ) was placed before the emission monochromator to eliminate polarization dependence of the detection train. Each data point on a lifetime decay curve represents the average of at least nine laser flashes, and each decay represents 300 of these data points evenly spaced over the collection time interval.

The fluorescence intensity decay data were analyzed by the multiexponential decay law, using the software supplied with the PTI instrument:

$$I(t) = \Sigma \alpha_i \exp(-t/\tau_i)$$

where I is fluorescence intensity, α_i and τ_i are the normalized preexponential factors, and decay time, respectively. The amplitude averaged lifetime $\langle\tau\rangle$ and the intensity averaged lifetime τ^{av} were calculated as $\langle\tau\rangle = \Sigma_i \alpha_i \tau_i$ and $\tau^{av} = \Sigma_i f_i \tau_i$ respectively. f_i, the fractional contribution of each lifetime component to steady-state fluorescence intensity, is defined as: $f_i = \frac{\alpha_i \tau_i}{\Sigma_j \alpha_j \tau_j}$

Accessibility of Trp side chain by acrylamide quenching of fluorescence

The fluorescence of a protein, monitored at the emission maximum λ_{max}, was quenched by the progressive addition of small aliquots of an 8M acrylamide solution as described elsewhere (37). Corrections for dilution of the sample and for inner filter effects caused by acrylamide absorption were performed as previously described (38). The quenching data were fit to the modified form of the Stern-Volmer relationship (38): $F_0/F = (1 + K_{sv}[Q]) \times e^{V[Q]}$ where F_0 and F are the fluorescence intensities in the absence and presence of the quencher, respectively, $[Q]$ is the concentration of quencher, V is the apparent static quenching constant (quenching sphere of action) and K_{SV} is the dynamic quenching constant ($K_{SV} = k_q \tau^{av}$), k_q is bimolecular collisional rate constant, and τ^{av} - is intensity averaged fluorescence lifetime in the absence of the quencher. It has been shown that the intensity averaged fluorescence lifetime should be used to calculate the average collisional quenching constant when the fluorophore displays multiexponential decay (39). The derived equation for the ratio of the amplitude averaged lifetimes in quenching is:

$$\frac{<\tau_0>_a}{<\tau>_a} = 1 + \Sigma f_i \tau_{0i} k_{qi} [Q] = 1 + K_{sv}^{av} [Q]$$

Where K_{sv}^{av} is an intensity averaged quenching constant. It should be emphasized that amplitude-, not intensity-, averaged lifetime is a linear function of steady-state fluorescence intensity. For dynamic component of quenching $\frac{F_0}{F} = \frac{<\tau_0>_a}{<\tau>_a}$. Therefore, use of intensity averaged lifetimes to calculate the average values of bimolecular collisional rate constants are clearly justified. The data were fit with the nonlinear least-squares method using OriginPro 8 software (OriginLab Corp., Northampton, MA).

Calculation of pK_a values from fluorescence λ_{max} data of single Trp mutant of TL

Data were analyzed with the assumption that pH-dependent changes in fluorescence λ_{max} are driven mainly by the ionization state of titratable amino acid side chains in close proximity of the tested Trp position. Data strongly support (see below) the validity of this assumption. Therefore, pH titration data were analyzed by fitting the function derived from the Henderson-Hasselbalch equation for multiple titratable groups (40):

$$\lambda_{obs}^{\max}=\lambda_{\min}^{\max}+\Sigma_i\frac{\Delta\lambda_i^{\max}\times 10^{(pH-pK_i)}}{1+10^{(pH-pK_i)}}$$

where $\lambda_{obs}^{\max}$ is the observed fluorescence λ_{max} value at any pH; $\lambda_{\min}^{\max}$ is the λ_{max} at the minimum pH value; $\Delta\lambda_i^{\max}$ is the fluorescence λ_{max} difference due to titration of the particular group (or groups with similar pK_a values) assigned by subscript. This equation assumes a noninteracting model with a rapid equilibrium between protonated and unprotonated groups. Data were fit to the above shown formula using OriginPro 8 software with the nonlinear least-squares method.

The side-chain pK_a values and free energy of unfolding of TL as a function of pH were calculated using the computer program PROPKA (41) using the coordinates of TL (PDB ID: 1XKI). Missing loop fragments (part of the loops AB and GH) were modeled using DeepView/Swiss-PdbViewer v.3.7 (GlaxoSmithKline R&D) in accord with solution structure data (2).

RESULTS AND DISCUSSION

The fluorescence quantum yield and the lifetime of Trp, as a free amino acid in solution, are invariant in the pH range between 3.0 and 8.5 (42,43). On the other hand, in proteins, fluorescence parameters of Trp are sensitive to the charge distribution around the indole ring. Therefore, Trp is an ideal “reporter” group to study the conformational changes within pH range of 3.0–8.5. TL shows pH-dependent ligand binding and conformational changes (23, 24,26). Specifically, pH regulates distance between the loops EF and CD in TL (24). However, the other two loops at the “open-end” of the barrel have not yet been investigated. Therefore, SDTF was applied to the loops AB and GH to interrogate pH induced conformational changes relevant to ligand binding. A single Trp residue, a reporter group, was introduced at various positions of TL as shown in Figure 1.

The side chain accessibility of the loops AB and GH residues in the low pH transition

Fluorescence parameters (intensity, λ_{max}, lifetimes, etc.) of Trp are sensitive to its immediate environment (45). Theoretical studies have predicted that upon excitation of Trp, electron density shifts from the pyrrole ring to the benzene ring (44). As a consequence, a positive charge near the benzene end or a negative charge near the pyrrole end of the Trp induces a red shift of fluorescence λ_{max} (44). Conversely, charges with opposite signs will generate a blue shift of fluorescence λ_{max}. Therefore, each Trp is expected to probe its microscopic electrostatic environment. The fluorescence λ_{max} values of single Trp mutants at pH values of 7.3 and 3.0 are shown in Figure 2A. In some positions, e.g., 25, 26, 27, 107, etc., the emission peaks are significantly blue shifted. Such hypsochromic shifts usually indicate decreased accessibilities (more buried) for the respective side chains of Trp. However, charged residues around the side chain of Trp may give a false impression of decreased accessibility. In any case, a significant shift in fluorescence λ_{max} indicates substantial changes in the environment of the Trp side chain. To detect conformational changes, which result in changes in accessibility to solvent molecules, experiments with acrylamide fluorescence quenching were performed at pH 7.3 and pH 3.0 (Figures 2B and 3). Bimolecular quenching constants, k_q, calculated from K_{SV} (see Material and Method), and fluorescence lifetime data are summarized in Table 1. The low pH

transition significantly changes fluorescence parameters of single Trp residues positioned in both loops. Fluorescence quantum yields and lifetimes are mostly decreased at pH 3.0 compared to that of pH 7.3. Qualitatively, this outcome can be understood from quenching properties of certain amino acids. Glu, Asp and His (pK_a values are 3.8, 4.5, and 6.5, respectively, in model compounds) are effective quenchers only in protonated states (46). Therefore, protonation of these side chains, which are in close proximity to the indole ring of Trp, will enhance fluorescence quenching. In the low pH transition, the changes in accessibility for the residues of the loops AB and GH are quite different. In the loop GH all residues show decreased accessibilities, which are consistent with transition to the "closed" conformation (Figure 2B). The fluorescence λ_{max} values follow the same pattern observed for the accessibility data. All Trp residues positioned in the loop GH show blue shifted emission in the low pH transition (Figure 2A). In contrast, the residues located in the loop AB show both decreased and increased accessibilities (Figure 2B). In the low pH transition, fluorescence λ_{max} values of Trp residues located in the loop AB show mostly blue shifted emission and have a somewhat different pattern than the accessibility data. Average accessibility of the residues in the loop GH is decreased about 38%, from 2.1×10^9 $M^{-1}s^{-1}$ to 1.3×10^9 $M^{-1}s^{-1}$, in the transition of pH from 7.3 to 3.0. However, in the same transition, despite the significant changes in accessibilities for some residues in the loop AB, the average accessibility per residue remained unchanged, average k_q= 1.2 $M^{-1}s^{-1}$ (from Table 1). The loop AB is the longest loop in the lipocalin family. Unlike the loop GH, conformational changes observed for the loop AB are not consistent with simple loop motion that just closes over the cavity. More likely, at pH 3.0 the loop assumes the conformation that reshuffles the accessibility profile of some residues. Previously, it has been noted that the loop AB could be a portal region and constituent of the excited protein states for ligand binding (15). The current findings suggest that various conformations of the loop AB in the excited protein states may be regulated by the protonation state of residues within and/or around that loop.

Global structural transition of TL in pH-titration

CD pH-titration experiments were performed to characterize global structural transitions of TL. Near-UV CD spectra of proteins are sensitive to both spatial arrangement and asymmetry (mobility) of its aromatic residues (47). Therefore, the near-UV CD spectrum is unique for each protein and reflects overall conformational state. The intensities of the near-UV CD spectrum of TL at λ=270, 277, 283 and 290nm as a function of pH are shown in Figure 4A. Decreased CD intensities indicate conformational relaxation of TL. Despite the fact that the contributions of the aromatic residues (Phe, Tyr, Trp) are different in selected wavelengths, all of them show a similar pattern and could be fit with global parameters. Two pK_a values, 3.7 and 5.2, are apparent from pH-titration in the near-UV CD (Figure 4A). The pH-titration experiment in far-UV CD yields similar pK_a values, 3.3 and 5.7 (Figure 4B). Concordance of pH-titration data in near- and far-UV CD indicates that the pH-induced structural transitions are cooperative. A previous CD study has shown that secondary structure of TL does not change significantly at pH 3.0 (24,26). However, near-UV CD of TL shows significantly diminished intensity at this pH value. ANS binding to TL at various pH values (7.5–2.0) shows that the ANS fluorescence enhancement reaches its maximum value at pH 3.0 and then sharply decreases (24). Enhanced ANS binding at low pH=3.0 is consistent with a molten globule transition (23,24,26). Therefore, pK_a values of 3.3–3.7, which were obtained from CD pH-titration experiments (Figure 4), can be considered as the pK_a for this transition. Decreased pH from 7.5 to 5.0 results in the enhanced near-UV CD intensities for TL (Figure 4A), which are suggestive of the more rigid conformations. It should be noted that there is an apparent disagreement between near- and far-UV CD results. Decrease of pH from 7.5 to 4.5 results in the diminished far-UV CD intensities (λ= 216 nm), which usually suggest unfolding of the protein. However, close inspection of the far-UV CD spectra of TL at various pH values (in reference (24)) shows that the apparent decrease of far-UV CD intensities are the result of an

overall spectral shift with almost the same spectral shape and intensity. As a result, ratio of the CD intensities, positive/negative, are increased. It has been shown that an increase of the degree of twist in β-sheets generates increased $|\theta_{\pi\pi}*|/|\theta_{n\pi}*|$, i.e., ratio of positive/negative peaks. This parameter have been suggested as a criterion for the degree of twisting in β-sheets (48). A right-hand twist of β-sheets lowers the free energy (49) and, therefore, increases stability of proteins. Thus, the pH titration data obtained from the far-UV CD corroborate that of the near-UV CD. The data suggest that TL undergoes a transition (pK_a about 5.7), which results in a more rigid conformation. The isoelectric point of TL is about 4.5–5.4 (32). The pH-titration data (Figure 4) indicate that more balanced charge distribution (pH value close to pI) enhances stability of TL. Unfolding free energies of TL at various pH values, calculated using PROPKA (41), match pH-titration data obtained with CD (Figure 4). In fact, both near-UV CD and PROPKA data could be fitted to a two-component pH-titration curve with pK_a values assigned as global parameters (Figure 4A). It is to be noted that neither near-UV CD nor far-UV CD is sensitive to the loop conformation unless it has secondary structure elements. Therefore, the results of pH-titration data of TL obtained by CD spectroscopy convey the global structural transitions associated with the secondary structure and are not specific for the particular part of the protein.

Site-specific pH-titration of TL by fluorescence of Trp positioned in the loops AB and GH

Fluorescence and accessibility parameters of Trp positioned in the loops AB and GH indicate conformational changes in the transit to low pH. CD spectroscopy reveals two global structural transitions (pK_a values about 3.5 and 5.7). However, the secondary structure of TL is essentially intact up to pH 3.5 (24). Since Trp fluorescence λ_{max} is most sensitive to its nearest charge distribution, pH-titration could reveal the mechanism of conformational transition in the loops. Fluorescence λ_{max} values of selected Trp residues as a function of pH for the loops AB and GH are shown in Figure 5 and 6, respectively. Because the fluorescence titration curves differ from each other, as well as from CD titration curves (Figure 4), the data strongly support that pH-titration curves are position dependent and, therefore, reflect the immediate environment of each Trp residue (Figures 5 and 6). PK_a values for each transition are shown in Table 2. For comparison, pK_a values of the titratable groups, as predicted by PROPKA are shown in Table 3. Up to three distinct pK_a values could be identified. Saturation of TL by palmitic acid (holo-proteins) generates significant changes to titration behavior of the amino acids around Trp 28 (Figure 5). Differences in protonation states between the holo- and apo-forms of the protein with single Trp in other positions are not apparent, with the exception of Trp37. Interestingly, both residues, position 28 and 37, are positioned in the flanking region of the loop AB. The data suggest that fluctuation of the protonation state around these residues (particularly around the residue 28) trigger conformational rearrangement of the loop AB that influences ligand binding. For the loop GH, no obvious shifts could be observed in pH titration curves between the holo- and apo-form of the proteins. Since variation in fluorescence λ_{max} values are linked to the accessibility data (Figure 2), vertical shift in the pH titration data could be associated with the amplitude of movement of the loops. While mutations of charged residues could disturb electrostatic interactions, native residues at positions 28 and 37 are uncharged residues, Phe and Thr,. Therefore, in the most significant case, the mutant Trp28 reports conformational changes where protonation states of adjacent residues are not perturbed. Regardless the nature of conformational transition of the loop AB, significant shift in pH titration curves apo- and holo-W28 indicates that the electrostatic interactions around this residue are stabilized by ligand binding and, therefore, functionally significant.

Note added after manuscript submission

The crystal structure of holo-TL (50), which became available after the submission of this manuscript, corroborates our findings. The spatial distributions of the relevant amino acids around the “reporter” Trp28 in apo-and holo-TL are informative (Figure 7). It has been

suggested that electrostatic contact between the residues Glu27 and Lys108, which are located in the neighboring loops AB and GH, fixes the “open” conformation of the loop AB for ligand binding (50). Indeed, in holo-TL the distance between amino acids Glu27 and K108 (OE1 and NA, respectively) decreases to 5.5 Å compared to that of apo-TL, 8.7 Å. The relative orientations and distances of the side chains of relevant amino acides around Trp 28 are noticeably different in holo- versus apo-TL (Figure 7). The significant difference between titration curves of apo-W28 and holo-W28 (Figure 5) found in solution corroborates findings from the crystal structures of apo- and holo-TL. Therefore, it is reasonable to suggest that fluctuations of the protonation states of these titratable groups, particularly E27, regulate ligand binding and define pH-dependence of the ligand binding. Because of complexity of the charge distribution, additional experimental data are necessary to assign the relative contributions of the titratible groups into the pH-titration curves of holo- and apo-W28. Previously, it has been shown that some mutations, notably E27W and K108W, decrease affinities of palmitic acid binding to TL (15). These results also corroborate the independently proposed mechanism (this manuscript and (50)). In both mutations, electrostatic interaction between residues E27 and K108, which fixes “open” conformation for ligand binding, will be disrupted.

The findings demonstrate that SDTF provides a promising approach to study the solution structure of proteins, as well as, pH-dependent conformational dynamics that is highly complementary to structural methods such as crystallography.

Acknowledgments

Supported by U.S. Public Health Service Grants NIH EY11224 and EY00331 as well as the Edith and Lew Wasserman Endowed Professorship in Ophthalmology.

Abbreviations

IRF	instrument response function
SDTF	site directed tryptophan fluorescence
TL	human tear lipocalin

REFERENCES

1. Flower DR. The lipocalin protein family: structure and function. Biochem J 1996;318(Pt 1):1–14. [PubMed: 8761444]
2. Gasymov OK, Abduragimov AR, Yusifov TN, Glasgow BJ. Site-directed tryptophan fluorescence reveals the solution structure of tear lipocalin: evidence for features that confer promiscuity in ligand binding. Biochemistry 2001;40:14754–14762. [PubMed: 11732894]
3. Breustedt DA, Korndorfer IP, Redl B, Skerra A. The 1.8-A crystal structure of human tear lipocalin reveals an extended branched cavity with capacity for multiple ligands. J Biol Chem 2005;280:484–493. [PubMed: 15489503]
4. Glasgow BJ, Abduragimov AR, Farahbakhsh ZT, Faull KF, Hubbell WL. Tear lipocalins bind a broad array of lipid ligands. Curr Eye Res 1995;14:363–372. [PubMed: 7648862]
5. Glasgow BJ, Marshall G, Gasymov OK, Abduragimov AR, Yusifov TN, Knobler CM. Tear lipocalins: potential lipid scavengers for the corneal surface. Invest Ophthalmol Vis Sci 1999;40:3100–3107. [PubMed: 10586930]
6. Selsted ME, Martinez RJ. Isolation and purification of bactericides from human tears. Exp Eye Res 1982;34:305–318. [PubMed: 7067743]
7. van't Hof W, Blankenvoorde MF, Veerman EC, Amerongen AV. The salivary lipocalin von Ebner's gland protein is a cysteine proteinase inhibitor. J Biol Chem 1997;272:1837–1841. [PubMed: 8999869]

8. Blaker M, Kock K, Ahlers C, Buck F, Schmale H. Molecular cloning of human von Ebner's gland protein, a member of the lipocalin superfamily highly expressed in lingual salivary glands. Biochim. Biophys. Acta 1993;1172:131–137. [PubMed: 7679926]
9. Redl B, Holzfeind P, Lottspeich F. cDNA cloning and sequencing reveals human tear prealbumin to be a member of the lipophilic-ligand carrier protein superfamily. J Biol Chem 1992;267:20282–20287. [PubMed: 1400345]
10. Lechner M, Wojnar P, Redl B. Human tear lipocalin acts as an oxidative-stress-induced scavenger of potentially harmful lipid peroxidation products in a cell culture system. Biochem J 2001;356:129–135. [PubMed: 11336644]
11. Glasgow BJ, Abduragimov AR, Gassymov OK, Yusifov TN, Ruth EC, Faull KF. Vitamin E associated with the lipocalin fraction of human tears. Adv Exp Med Biol 2002;506:567–572. [PubMed: 12613961]
12. Yusifov TN, Abduragimov AR, Gasymov OK, Glasgow BJ. Endonuclease activity in lipocalins. Biochem J 2000;347(Pt 3):815–819. [PubMed: 10769187]
13. Gasymov OK, Abduragimov AR, Yusifov TN, Glasgow BJ. Resolution of ligand positions by site-directed tryptophan fluorescence in tear lipocalin. Protein Sci 2000;9:325–331. [PubMed: 10716184]
14. Glasgow BJ, Gasymov OK, Abduragimov AR, Yusifov TN, Altenbach C, Hubbell WL. Side chain mobility and ligand interactions of the G strand of tear lipocalins by site-directed spin labeling. Biochemistry 1999;38:13707–13716. [PubMed: 10521278]
15. Gasymov OK, Abduragimov AR, Glasgow BJ. Intracavitary Ligand Distribution in Tear Lipocalin by Site-Directed Tryptophan Fluorescence. Biochemistry 2009;48:7219–7228. [PubMed: 19586017]
16. Okazaki K, Takada S. Dynamic energy landscape view of coupled binding and protein conformational change: induced-fit versus population-shift mechanisms. Proc Natl Acad Sci U S A 2008;105:11182–11187. [PubMed: 18678900]
17. Eberini I, Baptista AM, Gianazza E, Fraternali F, Beringhelli T. Reorganization in apo- and holo-beta-lactoglobulin upon protonation of Glu89: molecular dynamics and pKa calculations. Proteins 2004;54:744–758. [PubMed: 14997570]
18. Fogolari F, Ragona L, Licciardi S, Romagnoli S, Michelutti R, Ugolini R, Molinari H. Electrostatic properties of bovine beta-lactoglobulin. Proteins 2000;39:317–330. [PubMed: 10813814]
19. Ragona L, Fogolari F, Catalano M, Ugolini R, Zetta L, Molinari H. EF loop conformational change triggers ligand binding in beta-lactoglobulins. J Biol Chem 2003;278:38840–38846. [PubMed: 12857741]
20. Sakurai K, Konuma T, Yagi M, Goto Y. Structural dynamics and folding of beta-lactoglobulin probed by heteronuclear NMR. Biochim Biophys Acta 2009;1790:527–537. [PubMed: 19362581]
21. Fogolari F, Moroni E, Wojciechowski M, Baginski M, Ragona L, Molinari H. MM/PBSA analysis of molecular dynamics simulations of bovine beta-lactoglobulin: free energy gradients in conformational transitions? Proteins 2005;59:91–103. [PubMed: 15690343]
22. Prats M, Teissie J, Tocanne JF. Nature 1986;322:756–758.
23. Gasymov OK, Abduragimov AR, Glasgow BJ. Molten globule state of tear lipocalin: ANS binding restores tertiary interactions. Biochem Biophys Res Commun 2007;357:499–504. [PubMed: 17434452]
24. Gasymov OK, Abduragimov AR, Yusifov TN, Glasgow BJ. Interstrand loops CD and EF act as pH-dependent gates to regulate fatty acid ligand binding in tear lipocalin. Biochemistry 2004;43:12894–12904. [PubMed: 15461462]
25. Gasymov OK, Abduragimov AR, Gasimov EO, Yusifov TN, Dooley AN, Glasgow BJ. Tear lipocalin: potential for selective delivery of rifampin. Biochim. Biophys. Acta 2004;1688:102–111. [PubMed: 14990340]
26. Gasymov OK, Abduragimov AR, Yusifov TN, Glasgow BJ. Structural changes in human tear lipocalins associated with lipid binding. Biochim Biophys Acta 1998;1386:145–156. [PubMed: 9675263]
27. Calderone V, Berni R, Zanotti G. High-resolution structures of retinol-binding protein in complex with retinol: pH-induced protein structural changes in the crystal state. J Mol Biol 2003;329:841–850. [PubMed: 12787682]

28. Newcomer ME, Ong DE. Plasma retinol binding protein: structure and function of the prototypic lipocalin. Biochim Biophys Acta 2000;1482:57–64. [PubMed: 11058747]
29. Roberts SA, Weichsel A, Qiu Y, Shelnutt JA, Walker FA, Montfort WR. Ligand-induced heme ruffling and bent no geometry in ultra-high-resolution structures of nitrophorin 4. Biochemistry 2001;40:11327–11337. [PubMed: 11560480]
30. Hwang PM, Choy WY, Lo EI, Chen L, Forman-Kay JD, Raetz CR, Prive GG, Bishop RE, Kay LE. Solution structure and dynamics of the outer membrane enzyme PagP by NMR. Proc Natl Acad Sci U S A 2002;99:13560–13565. [PubMed: 12357033]
31. Glasgow BJ, Heinzmann C, Kojis T, Sparkes RS, Mohandas T, Bateman JB. Assignment of tear lipocalin gene to human chromosome 9q34-9qter. Curr Eye Res 1993;12:1019–1023. [PubMed: 8306712]
32. Glasgow BJ. Tissue expression of lipocalins in human lacrimal and von Ebner's glands: colocalization with lysozyme. Graefes Arch Clin Exp Ophthalmol 1995;233:513–522. [PubMed: 8537027]
33. Cormack, B. In Current Protocol in Molecular Biology. Vol. Vol. suppl. 15. Greene Pub. Associates and Wiley- Interscience; New York, N.Y.: 1987.
34. Gasymov OK, Abduragimov AR, Yusifov TN, Glasgow BJ. Binding studies of tear lipocalin: the role of the conserved tryptophan in maintaining structure, stability and ligand affinity. Biochim Biophys Acta 1999;1433:307–320. [PubMed: 10515687]
35. Bozimowski D, Artiss JD, Zak B. The variable reagent blank: protein determination as a model. J Clin Chem Clin Biochem 1985;23:683–689. [PubMed: 4067517]
36. Peterson GL. A simplification of the protein assay method of Lowry et al. which is more generally applicable. Anal Biochem 1977;83:346–356. [PubMed: 603028]
37. Gasymov OK, Abduragimov AR, Yusifov TN, Glasgow BJ. Solution structure by site directed tryptophan fluorescence in tear lipocalin. Biochem Biophys Res Commun 1997;239:191–196. [PubMed: 9345294]
38. Eftink MR, Ghiron CA. Exposure of tryptophanyl residues in proteins. Quantitative determination by fluorescence quenching studies. Biochemistry 1976;15:672–680. [PubMed: 1252418]
39. Sillen A, Engelborghs Y. The Correct Use of “Average” Fluorescence Parameters. Photochem Photobiol 1998;67:475–486.
40. Freedman MH, Lyerla JR Jr. Chaiken IM, Cohen JS. Carbon-13 nuclear-magnetic-resonance studies on selected amino acids, peptides, and proteins. Eur J Biochem 1973;32:215–226. [PubMed: 4631542]
41. Li H, Robertson AD, Jensen JH. Very fast empirical prediction and rationalization of protein pKa values. Proteins 2005;61:704–721. [PubMed: 16231289]
42. De Lauder WB, Wahl P. pH dependence of the fluorescence decay of tryptophan. Biochemistry 1970;9:2750–2754. [PubMed: 5450239]
43. Liu B, Thalji RK, Adams PD, Fronczek FR, McLaughlin ML, Barkley MD. Fluorescence of cis-1-amino-2-(3-indolyl)cyclohexane-1-carboxylic acid: a single tryptophan chi(1) rotamer model. J Am Chem Soc 2002;124:13329–13338. [PubMed: 12405862]
44. Vivian JT, Callis PR. Mechanisms of tryptophan fluorescence shifts in proteins. Biophys J 2001;80:2093–2109. [PubMed: 11325713]
45. Lakowicz, JR. Principles of Fluorescence Spectroscopy. Vol. Third ed.. Springer; New York: 2006.
46. Chen Y, Barkley MD. Toward understanding tryptophan fluorescence in proteins. Biochemistry 1998;37:9976–9982. [PubMed: 9665702]
47. Fasman, GD., editor. Circular dichroism and the conformational analysis of biomolecules. Plenum Press; New York: 1996.
48. Woody, RW. Theory of Circular Dichroism of Proteins. In: Fasman, GD., editor. Circular Dichroism and the Conformational Analysis of Biomolecules. Plenum Press; New York: 1996. p. 55
49. Chothia C. Conformation of twisted beta-pleated sheets in proteins. J Mol Biol 1973;75:295–302. [PubMed: 4728692]
50. Breustedt DA, Chatwell L, Skerra A. A new crystal form of human tear lipocalin reveals high flexibility in the loop region and induced fit in the ligand cavity. Acta Crystallogr D Biol Crystallogr 2009;65:1118–1125. [PubMed: 19770509]

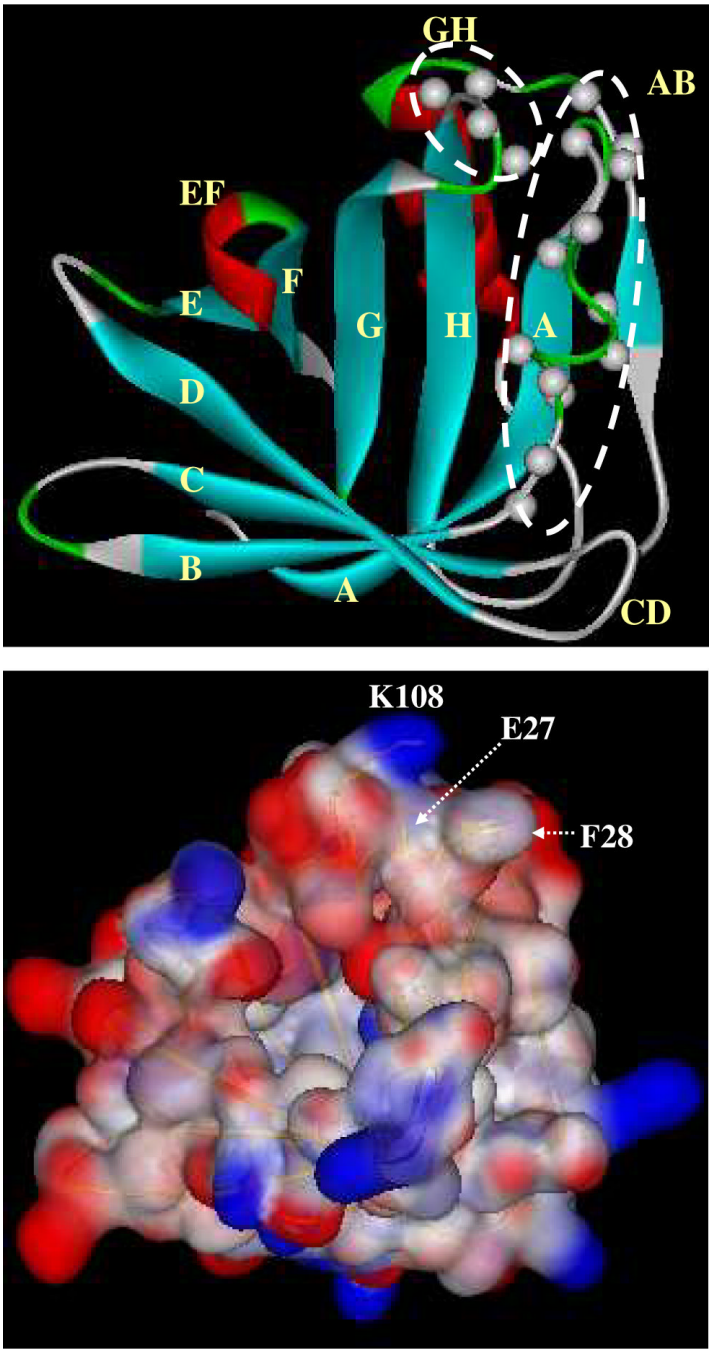

Figure 1.

Positions of the residues in the loop AB and GH that were sequentially substituted with Trp to examine pH induced conformational changes in TL. Gray balls show locations of the C_α atoms of the amino acid residues. Dashed lines encompass the inspected loop regions. Single and double letters denote the identities of the β-strands and loops, respectively. The ribbon diagram (blue, β-strands; red, α-helix; green, turns; gray, loops) of TL was generated from PDB 1XKI with DS Visualizer 2.0 (Accelrys Inc.). Missing loop fragments (part of the loops AB and GH) were modeled using DeepView/Swiss-PdbViewer v.3.7 (GlaxoSmithKline R&D) in accord with solution structure data (2). Lower figure: surface representation of tear lipocalin, in the

same orientation as in upper lane, (colored according to the electrostatic potential: blue, positive charge; red, negative charge).

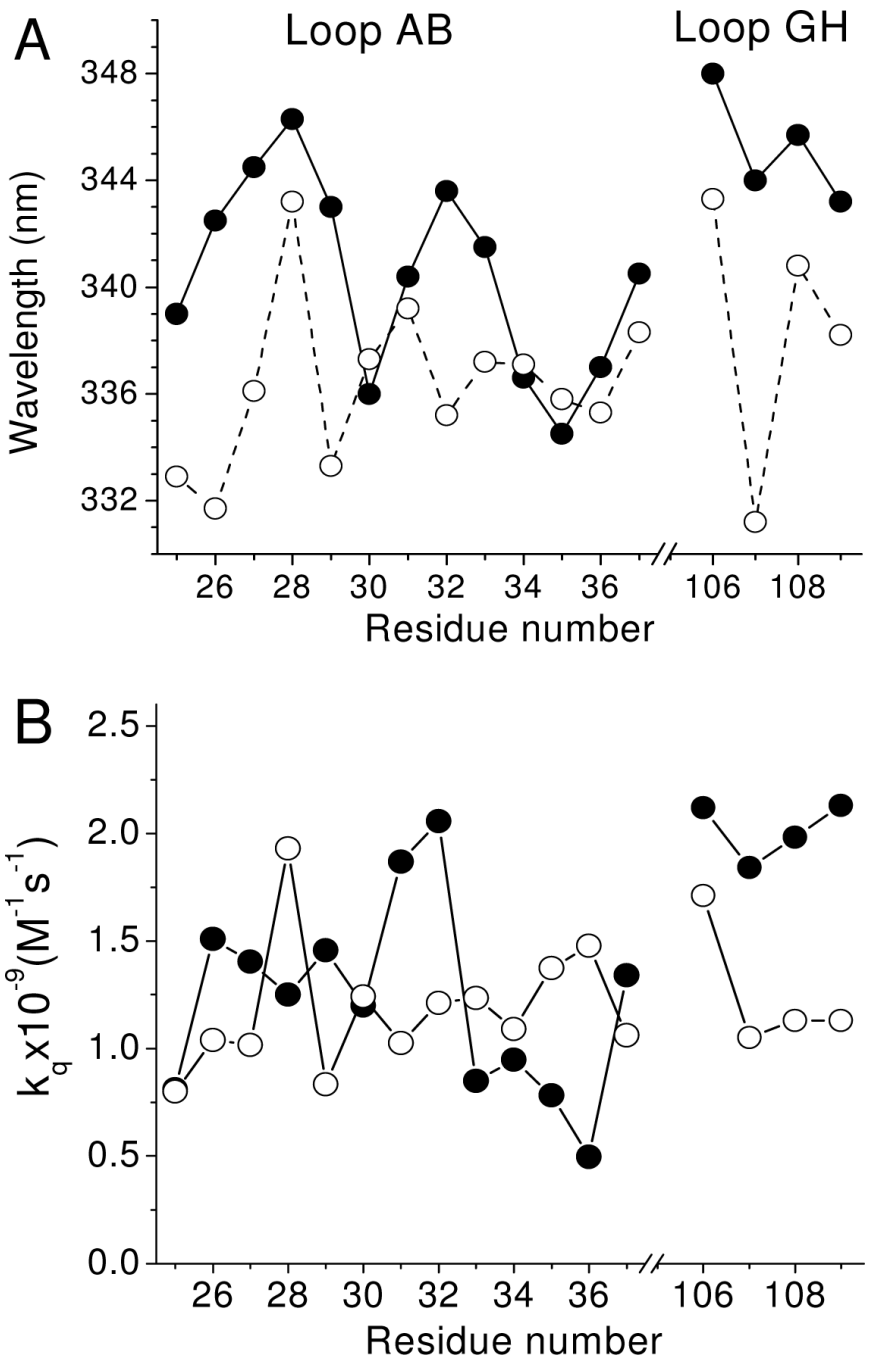

Figure 2.

Fluorescence λ_{max} (A) and bimolecular quenching rate constants (acrylamide) (B) for the single Trp positioned in the loops AB and GH at pH values of 7.3 (solid circles) and 3.0 (open circles). Fluorescence λ_{max} values are determined from the corrected spectra.

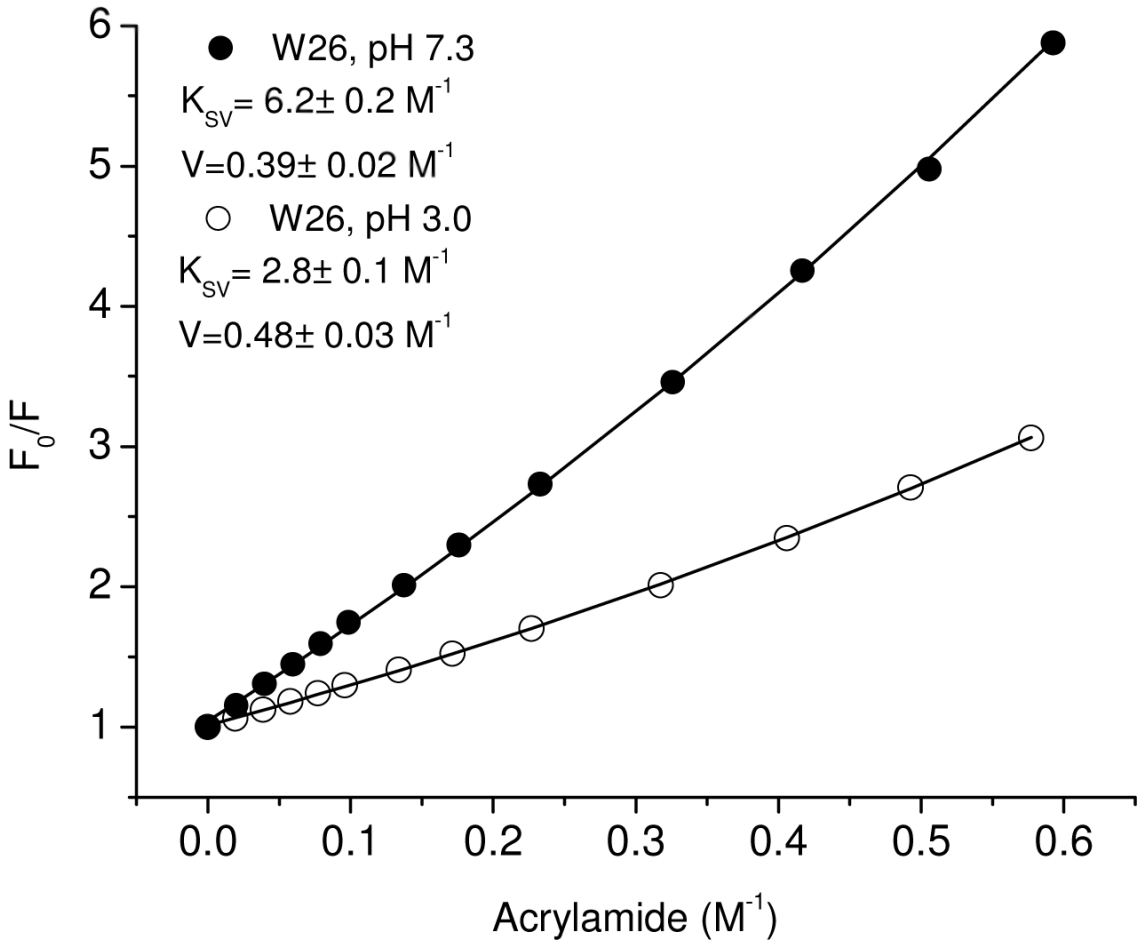

Figure 3.
Acrylamide quenching of single Trp mutant of TL (W26 as an example) at pH 7.3 and 3.0.

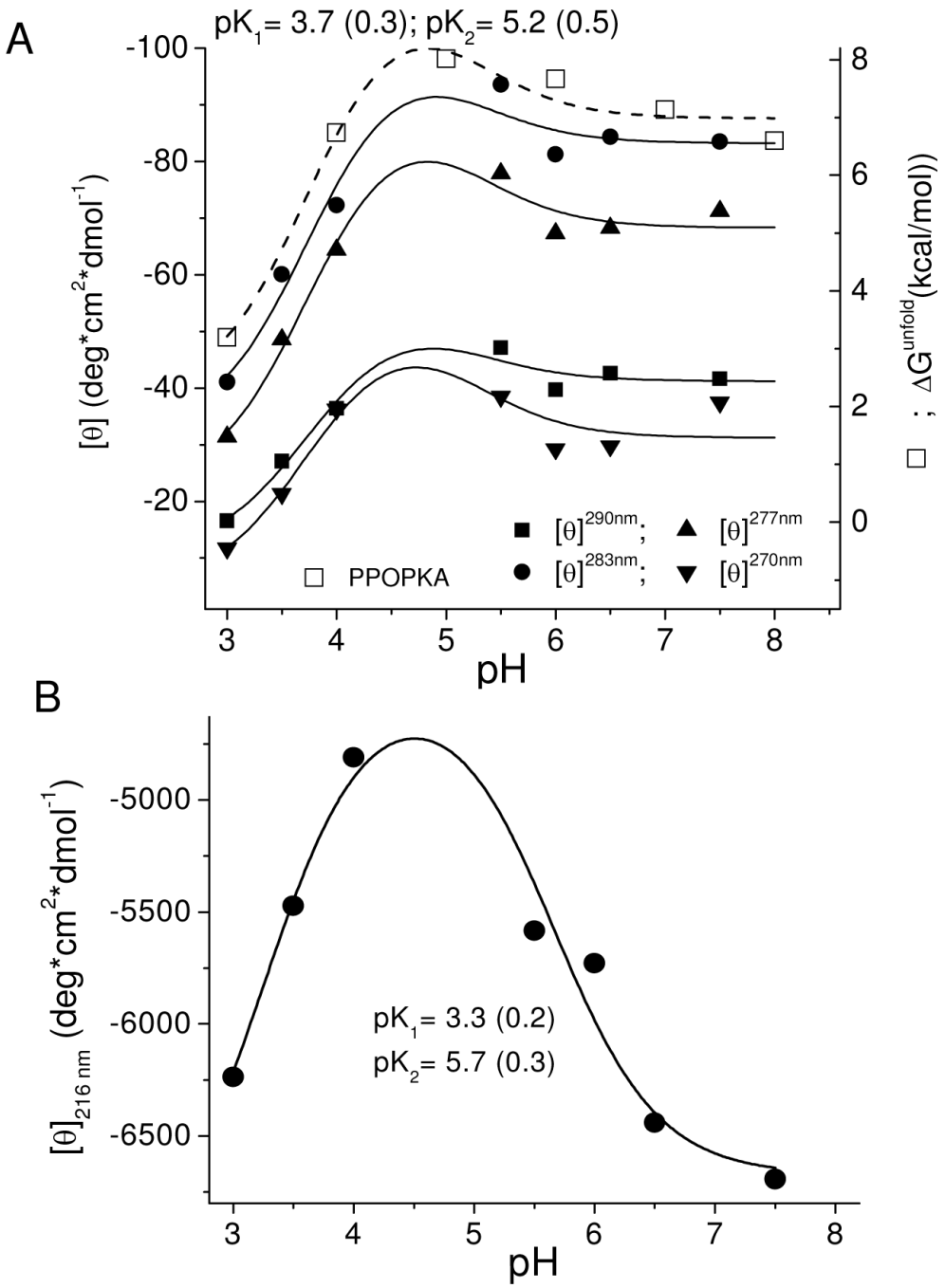

Figure 4.

(A) Molar ellipticities at λ= 270, 277, 283 and 290nm (from near-UV CD) and free energy unfolding (calculated using PROPKA) for TL at various pH values. Lines are generated by a global analysis of the data with a two-component pH titration curve where pK values are assigned as global parameters. (B) Molar ellipticity at λ= 216 nm (from far-UV CD) for TL at various pH values. CD data points are from reference (24).

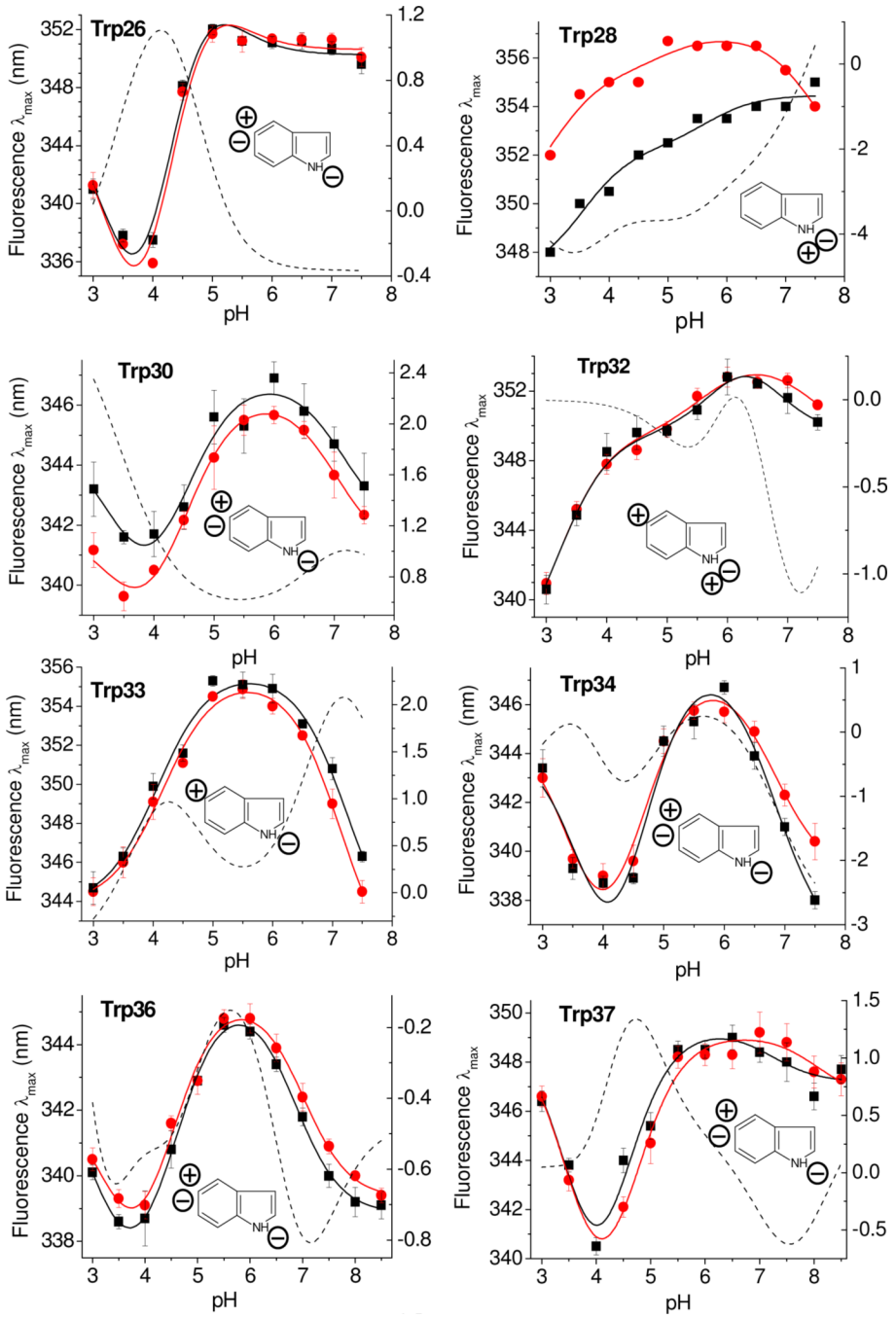

Figure 5.

Fluorescence λ_{max} data as a function of pH for single Trp mutants of the loop AB. Red and black symbols represent apo- and holo-proteins, respectively. Solid lines are fitting curves for two or three titratable groups (see Materials and Methods). Dashed lines (right-side scale) are difference titration curves (holoapo). In order to eliminate additional uncertainty in titration experiments, fluorescence λ_{max} values are taken from the uncorrected (only corrected for buffer scattering) spectra. Inset, pictures represent models for apparent charge distributions around the indole ring of Trp consistent with experimental data. pK_a values above 5.0 were modeled as a positive charge. Effect of charged group (positive or negative) localized around indole ring on fluorescence λ_{max} described in the text.

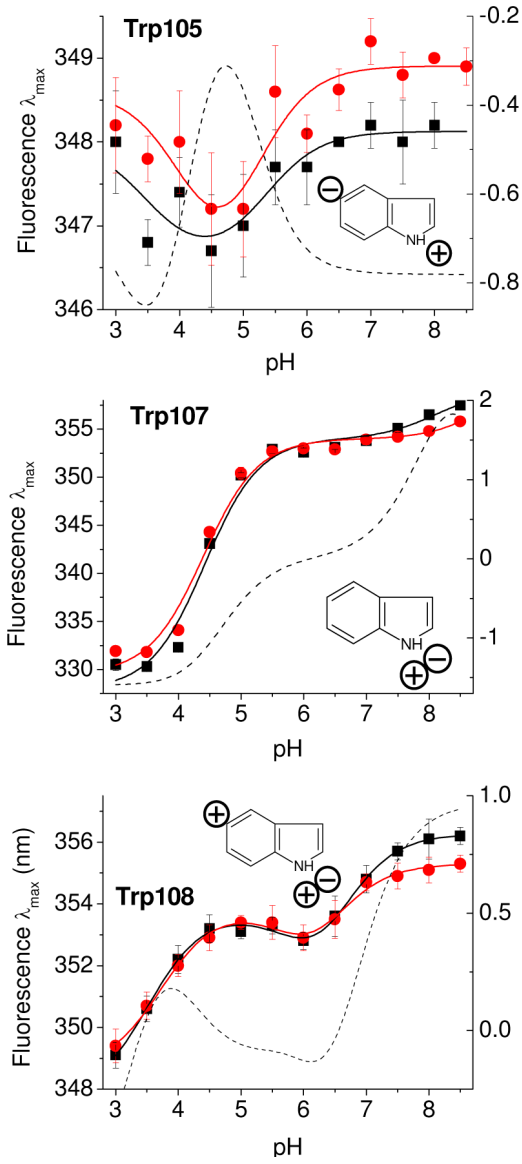

Figure 6.

Fluorescence λmax data as function of pH for single Trp mutants of the loop GH. Red and black symbols represent apo- and holo-proteins, respectively. Solid lines are fitting curves for two or three titratable groups (see Materials and Methods). Dashed lines (right side scale) are difference titration curves (holoapo). Inset, same as in Figure 5.

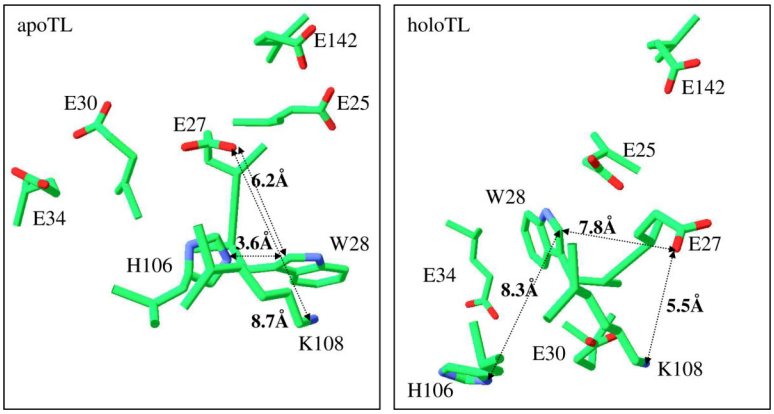

Figure 7.

Distribution of relevant charged residues around Trp 28 (F28W mutant) in apoand holo TL, coordinates of which were taken from PDB entries 1XKI and 3EYC, respectively. Molecules were superimposed using the software DeepView/Swiss-PdbViewer v.3.7 (GlaxoSmithKline R&D), which included 109 atoms (RMS: 1.2 Å). Color-coding: green, backbone and carbon atoms; red, oxygen; blue, nitrogen.

Table 1

Fluorescence lifetime parameters for single Trp mutants of TL.

Trp Mutant	α_1	α_2	τ_1 (ns)	τ_2 (ns)	τ_{aver} (ns)	$\langle\tau\rangle$ (ns)	K_{SV} (M^{-1})	$k_q \times 10^{-9}$ ($M^{-1}s^{-1}$)	V (M^{-1})	Q	χ^2
W25, pH 7.3	0.49	0.51	2.10	5.16	4.30	3.66	3.5	0.81	0.18	0.10	1.1
W25, pH 3.0	0.62	0.38	1.17	4.20	3.26	2.32	2.6	0.80	0.62	0.08	1.3
W26, pH 7.3	0.62	0.38	2.12	5.39	4.11	3.36	6.2	1.51	0.39	0.11	1.0
W26, pH 3.0	0.65	0.35	0.80	3.48	2.68	1.74	2.8	1.04	0.48	0.08	1.6
W27, pH 7.3	0.37	0.63	1.57	6.34	5.73	4.58	8	1.40	0.72	0.15	1.1
W27, pH 3.0	0.68	0.32	1.11	4.03	2.95	2.04	3.0	1.02	0.67	0.07	1.5
W28, pH 7.3	0.40	0.60	0.93	4.50	4.07	3.07	5.1	1.25	0.79	0.13	1.1
W28, pH 3.0	0.64	0.36	0.84	3.49	2.70	1.79	5.2	1.93	0.94	0.07	1.4
W30, pH 7.3	0.65	0.35	0.80	3.38	2.59	1.70	3.1	1.20	0.35	0.07	1.0
W30, pH 3.0	0.74	0.26	1.42	4.16	2.82	2.13	3.5	1.24	0.94	0.07	1.8
W31, pH 7.3	0.68	0.32	1.05	4.12	3.05	2.03	5.7	1.87	0.66	0.10	1.6
W31, pH 3.0	0.69	0.31	1.13	3.80	2.73	1.96	2.8	1.03	1.35	0.06	1.1
W32, pH 7.3	0.65	0.35	1.24	4.69	3.55	2.45	7.3	2.06	0.65	0.11	1.2
W32, pH 3.0	0.62	0.38	0.94	3.80	2.97	2.03	3.6	1.21	1.29	0.08	1.5
W33, pH 7.3	0.50	0.50	1.19	3.70	3.09	2.45	2.8	0.91	0.47	0.10	1.0
W33, pH 3.0	0.67	0.33	0.85	3.57	2.67	1.75	3.3	1.24	1.58	0.07	1.9
W34, pH 7.3	0.43	0.57	0.92	3.83	3.38	2.58	3.6	1.07	0.3	0.12	1.2
W34, pH 3.0	0.77	0.23	1.54	5.05	3.30	2.35	3.6	1.09	0.64	0.08	1.2
W35, pH 7.3	0.27	0.73	1.10	4.28	4.00	3.42	3.2	0.80	0.29	0.13	0.9
W35, pH 3.0	0.60	0.40	1.24	4.55	3.59	2.56	4.9	1.36	0.63	0.12	0.7
W36, pH 7.3	0.45	0.55	1.40	4.73	4.08	3.23	1.8	0.44	0.43	0.12	1.1
W36, pH 3.0	0.74	0.26	1.34	4.21	2.83	2.09	4.2	1.48	0.66	0.08	1.0
W37, pH 7.3	0.65	0.35	0.77	3.89	3.05	1.86	4.1	1.34	0	0.02	1.1
W37, pH 3.0	0.66	0.34	1.19	4.39	3.30	2.28	3.5	1.06	0.84	0.07	1.8
W106, pH 7.3	0.38	0.62	1.16	3.56	3.16	2.65	6.7	2.12	0.81	0.10	0.9
W106, pH 3.0	0.59	0.41	1.01	3.33	2.63	1.96	4.5	1.71	0	0.07	1.3
W107, pH 7.3	0.44	0.56	1.08	5.07	4.50	3.31	8.1	1.80	0.6	0.12	0.9
W107, pH 3.0	0.83	0.17	0.80	3.41	2.00	1.24	2.1	1.05	0	0.06	1.8
W108, pH 7.3	0.41	0.59	0.80	4.55	4.14	3.01	8.8	2.13	0.14	0.10	1.0

Trp Mutant	α_1	α_2	τ_1 (ns)	τ_2 (ns)	τ_{aver} (ns)	$\langle\tau\rangle$ (ns)	K_{SV} (M^{-1})	$k_q \times 10^{-9}$ ($M^{-1}s^{-1}$)	V (M^{-1})	Q	χ^2
W108, pH 3.0[a]	0.50;0.41	0.08	0.47;2.16	5.64	2.92	1.58	3.3	1.13	0	0.07	1.3

[a] 3 lifetime components were necessary for sufficient fitting.

Table 2

pK_a values for apo- and holo-forms of single Trp mutants of TL determined from fluorescence pH-titration data (Figures 5 and 6)

Mutant proteins	pK_{a1} ± s.d.	pK_{a2} ± s.d.	pK_{a3} ± s.d.
apoW26	3.5[a]	4.3 ± 0.5	4.9 ± 0.8
holoW26	3.5[a]	4.3 ± 0.5	5.0 ±0.8
apoW28	3.0 ± 0.3	4.9 ± 1.2	7.5 ± 1.0
holoW28	3.5 ± 0.2	5.7 ± 0.6	-
apoW30	3.4 ± 0.3	4.5 ± 0.2	7.0 ± 0.4
holoW30	3.4 ± 0.3	4.5 ± 0.3	7.1 ± 0.4
apoW32	3.2 ± 0.2	5.6 ± 0.4	7.4 ± 1.2
holoW32	3.2 ± 0.2	6.0 ± 1.1	6.6 ± 1.1
apoW33	-	4.2 ± 0.1	7.1 ± 0.2
holoW33	-	4.1 ± 0.1	7.3 ± 0.2
apoW34	3.6 ± 0.4	4.5 ± 0.4	6.8 ± 0.4
holoW34	3.9 ± 0.6	4.4 ± 0.6	6.8 ± 0.3
apoW36	3.3 ± 0.6	4.5 ± 0.2	7.0 ± 0.1
holoW36	3.0 ± 0.8	4.6 ± 0.2	6.9 ± 0.1
apoW37	3.6 ± 0.3	4.6 ± 0.3	8.0 ± 1.0
holoW37	3.6 ± 0.3	4.4 ± 0.4	7.2 ± 0.7
apoW105	4.1 ± 0.6	5.1 ± 0.6	-
holoW105	3.5 ± 0.5	5.3 ± 0.5	-
apoW107	-	4.4 ± 0.1	8.9[b] ± 6.4
holoW107	-	4.4 ± 0.1	8.1 ± 1.1
apoW108	3.7 ± 0.1	6.2 ± 1.6	6.2 ± 0.5
holoW108	3.5 ± 0.1	6.2 ± 1.6	6.4 ± 1.0

[a] fixed value

[b] low accuracy value

Table 3

pK_a values of titratable groups relevant ligand binding for TL as predicted by the software PROPKA*.

Amino Acid	pK_a(apo) PROPKA	pK_a model
Asp25	3.21	3.8
Glu27	4.61	4.50
Glu30	6.44	4.50
Glu34	3.85	4.50
Glu102	3.91	4.50
Glu104	4.89	4.50
Glu142	5.37	4.50
His84	10.26	6.50
His96	7.51	6.50
His106	6.29	6.50

* The atomic coordinates for calculations of pK_a values were taken from PDB: 1xki.